Luminescent Iridium Complex with a Sulfurated Bipyridine Ligand: PCET Thermochemistry of the Disulfide Unit and Photophysical Properties

Manuel Oelschlegel,[†] Shao-An Hua,[†] Lucius Schmid,[#] Philipp Marquetand,[‡] Anna Bäck,[‡] Jan-Hendrik Borter,[§] Jana Lücken,[†] Sebastian Dechert,[†] Oliver S. Wenger,[#] Inke Siewert,[†,$] Dirk Schwarzer,[§,*] Leticia González[‡,*] and Franc Meyer[†,*,$]

[†] University of Göttingen, Institute of Inorganic Chemistry, Tammannstr. 4, D-37077 Göttingen, Germany

[‡] University of Vienna, Institute of Theoretical Chemistry, Währingerstraße 17, A-1090 Vienna, Austria

[§] Department of Dynamics at Surfaces, Max-Planck-Institute for Multidisciplinary Sciences, Am Faßberg 11, D-37077 Göttingen, Germany

[#] University of Basel, Department of Chemistry, CH-4056 Basel, Switzerland

[$] International Center for Advanced Studies of Energy Conversion (ICASEC), D-37077 Göttingen, Germany

ABSTRACT: Molecular systems combining light harvesting and charge storage are receiving great attention in the context of, e.g., artificial photosynthesis and solar fuel generation. As part of ongoing efforts to develop new concepts for photoinduced proton-coupled electron transfer (PCET) reactivities, we report a cyclometallated iridium(III) complex **[1]**$^+$ equipped with our previously developed sulfurated bipyridine ligand $^{S-S}$bpy. A new one-step synthetic protocol for $^{S-S}$bpy is developed, starting from commercially available 2,2'-bipyridine, which significantly facilitates the use of this ligand. The iridium complex [Ir(ppy)$_2$($^{S-S}$bpy)](PF$_6$) (**[1]**PF$_6$) features a two-electron reduction with potential inversion ($|E_1|>|E_2|$) at moderate potentials (E_1 = –1.17, E_2 = –1.08 V *vs.* Fc$^{+/0}$ at 253 K), leading to a dithiolate species **[1]**$^-$. Protonation with weak acids allows for determination of pK_a = 23.5 in MeCN for the S–H··S$^-$ unit of **[1]**H. The driving forces for both H atom and hydride transfer are calculated to be ~60 kcal mol^{-1} and verified experimentally by reaction with suitable H atom and a hydride acceptors, demonstrating the ability of **[1]**$^+$ to serve as a versatile PCET reagent, albeit with limited thermal stability. In MeCN solution, an orange emission for **[1]**PF$_6$ from a triplet excited state was found. Density functional calculations and ultrafast absorption spectroscopy are used to give insight into the excited-state dynamics of the complex and suggest a significantly stretched S–S bond for lowest triplet state T_1. The structural responsiveness of the disulfide unit is proposed to open an effective relaxation channel towards the ground state, explaining the unexpectedly short lifetime of **[1]**$^+$. These insights as well as the quantitative ground-state thermochemistry data provide valuable information for the use of $^{S-S}$bpy functionalized complexes and their disulfide/dithiol directed PCET reactivity.

INTRODUCTION

Similar to natural photosynthesis, most of the reactions relevant to artificial solar fuel generation –including water oxidation, proton or CO_2 reduction, or conversion of N_2 to NH_3– involve the synchronized transfer of multiple protons and electrons. In order to integrate such proton-coupled electron transfer (PCET) processes with light absorption and excited state reactivity in photocatalytic schemes,[1–5] one promising approach is to equip the ligands of common metal-based photosensitizers with e$^-$/H$^+$ storage sites for triggering PCET after metal-to-ligand charge transfer (MLCT) excitation.[6–8] As an important further advance these units should be able to accumulate redox equivalents and protons for mediating chemical multi-e$^-$/H$^+$ conversions. Prominent examples are the polypyridyl ruthenium complexes with NAD$^+$/NADH-type ligands developed by Tanaka and co-workers, whose NAD$^+$ form can undergo light-triggered 2e$^-$/2H$^+$ reduction;[9–11] such systems have been used for, e.g. selective hydride transfer to CO_2.[12] In that context we recently introduced a new 2,2'-bipyridine (bpy) derivative equipped with a peripheral disulfide unit, in the following abbreviated as $^{S-S}$bpy (Figure 1).[13] This molecule was shown to be capable of 2e$^-$ redox processes by exploiting the disulfide/dithiolate couple, which tends to be coupled to (de) protonation events and is reminiscent of disulfide/dithiol based biological charge storage.[14] In-depth electrochemical investigation revealed that reduction of $^{S-S}$bpy accompanied by protonation induces potential inversion, viz. the second reduction is thermodynamically more favored than the first one,[15,16] hence leading to a preferred 2e$^-$ reduction forming a dithiolate from a disulfide, in this case. The concept of potential inversion for the disulfide-dithiolate interchange has recently been ex-

ploited for light-driven charge accumulation and multielectron catalysis in a molecular donor–sensitizer–acceptor compound without any sacrificial reagents.[2]

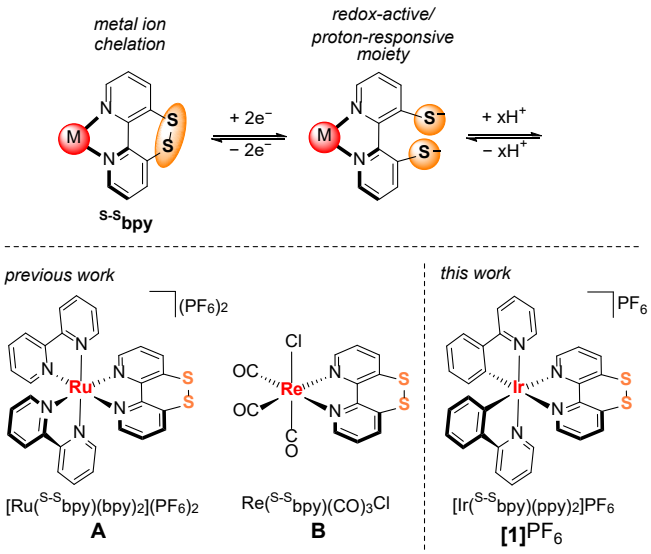

Figure 1. Concept of the ligand $^{S-S}$bpy as a multi-PCET unit (top); previously reported and new complexes of $^{S-S}$bpy (bottom).[17,18]

The first reported complex of $^{S-S}$bpy, $[Ru(bpy)_2(^{S-S}bpy)]^{2+}$ (**A** in Figure 1), was shown to undergo 2e⁻ reduction centered on the disulfide moiety.[17] While the free ligand exhibits potential inversion only in the presence of protons, it does so when *N*,*N*'-chelating a metal ion in **A**,[17] and the two potentials were found to be equal in rhenium(I) complex **B**.[18] After injection of the second electron, the disulfide bond breaks to form the corresponding dithiolate; however, in case of **A** it was observed that reduction triggers sulfide extrusion from $^{S-S}$bpy to give *N*,*N*'-chelating thieno[3,2-b:4,5-b']bipyridine. To better understand the ground-state PCET thermodynamics of $^{S-S}$bpy coordinated to a metal ion, specifically the reduction potentials and the protonation behavior, we used complex **B** that does not exhibit the drawback of rapid decomposition of the reduced species at room temperature. It was found that upon two-electron reduction at moderate potentials ($E_1 = E_2 = -1.17$ V *vs.* $Fc^{+/0}$) in acetonitrile (MeCN) solution, the resulting dithiolate can be protonated once with a pK_a of 24.3.[18] The resulting doubly reduced and singly protonated S–H···S⁻ complex can act as a formal hydride donor with a hydricity of 60 kcal mol⁻¹, similar to synthetic analogues of biological hydride transfer reagents such as nicotinamide adenine dinucleotide (NAD^+|NADH).[18,19] In addition, H atom transfer (HAT) of the S–H···S⁻ complex is also possible (BDEF(S–H) = 59 kcal mol⁻¹), demonstrating the rich and versatile PCET chemistry which can originate from the peripheral disulfide functional group.

Additionally, **A** can be selectively excited into a ^{3}MLCT state with high charge transfer character localized on the $^{S-S}$bpy ligand, where the electron ends up on in less than 80 fs.[20] The selective excitation makes it a promising candidate for excited-state reactivity involving the reactive disulfide. However, the complex exhibits a low-energy emission centered at only 730 nm (1.7 eV). In order to gain more driving force for excited-state reactions, a higher emission energy is highly desirable. Since cyclometallated iridium(III) complexes tend to be more oxidizing after photoexcitation,[21] we concluded that a sulfurated derivative of the popular $[Ir(ppy)_2(bpy)]^+$ photosensitizer (Hppy = 2-phenylpyridine), whose photophysics has been studied in great detail,[22–24] should be a promising target. Cyclometallated iridium chromophores are among the most prominent classes of photosensitizers[25,26] and have proven to be suitable for, e.g., photoredox catalysis,[27,21] organic light-emitting devices[28] or luminescent sensors.[29,30] As a synthetic benefit, the sequential installing of the cyclometallating and ancillary ligands in two separate synthetic steps offers synthetic versatility for such iridium(III) complexes.[25]

In this study, we now present a first iridium complex of $^{S-S}$bpy, $[Ir(ppy)_2(^{S-S}bpy)](PF_6)$ (**[1]**PF_6; Figure 1 bottom), and we have investigated both experimentally and computationally its photophysical properties as well as the ground-state thermochemistry related to the peripheral disulfide/dithiol interconversion. In particular, by comparing results for **B** and **[1]**⁺ we wanted to see how the PCET thermodynamics is affected by different metal ion templates the $^{S-S}$bpy ligand is bound to.

RESULTS AND DISCUSSION

Improved synthesis of the ligand $^{S-S}$bpy. So far, the use of $^{S-S}$bpy in coordination chemistry and the exploitation of its 2e⁻/xH⁺ interconversions were severely hampered by its low-yielding multi-step synthesis (<2% overall yield, Scheme 1, top), which also gave side-products that are difficult to separate.[13] In general, disulfides can be synthesized by aerobic oxidation of the corresponding (di-)thiols,[21,31] for which not many generally applicable synthetic methods are known. Prominent methods include the nucleophilic substitution with xanthates[32] or the Newman-Kwart-rearrangement[33] followed by (reductive) cleavage of the carbamate/dithiocarbonate.[34] While nucleophilic substitution at heterocycles is easier than at parent phenyl groups, the 3,3'-positions of 2,2'-bipyridine are not particularly activated, and the Newman-Kwart-rearrangement is difficult in heteroaromatic systems.[13,33] Thus, in the present study we aimed at developing a new synthetic strategy to facilitate the use of $^{S-S}$bpy and related disulfurated ligand platforms.

Inspired by two reported synthetic methods,[35,36] we now established a new one-step protocol that involves the double deprotonation of 2,2'-bipyridine with Li[TMP] (HTMP = 2,2',6,6'-tetramethylpiperidine) in THF at −78 °C followed by quenching of the lithiated species with elemental sulfur, as shown in Scheme 1, bottom. The N-atoms serve as directing group for the regioselective deprotonation at the 3/3' positions.

Scheme 1. Previous[13] and new synthetic route to the ligand $^{S-S}$bpy.

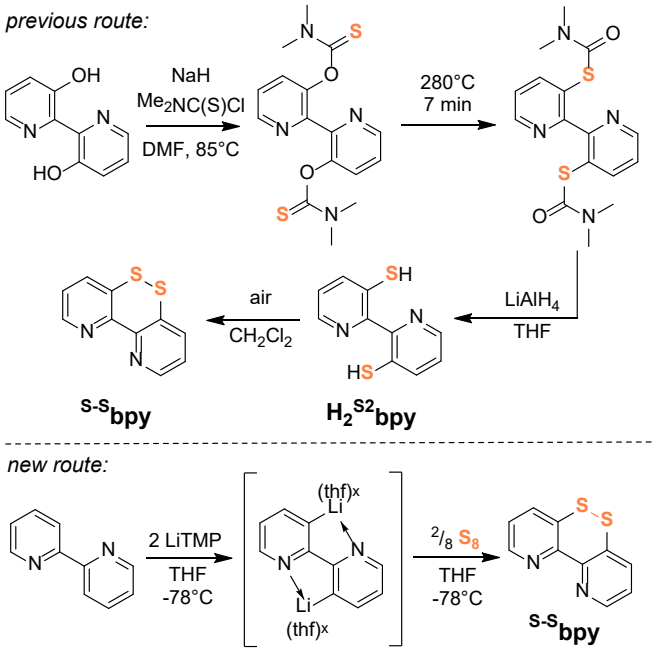

After separation of the crude reaction mixture by column chromatography, $^{S-S}$bpy is obtained as a yellow-brown solid with a moderate yield of 23%, which represents a significant improvement over the previous synthesis. Spectroscopic data of the product are in good agreement with the published ones for $^{S-S}$bpy,[13] and the purity was confirmed by combustion analysis. Single crystals of $^{S-S}$bpy suitable for X-ray diffraction could be grown by slow evaporation of a dichloromethane solution. The unit cell contains two crystallographically independent molecules with similar bond lengths and angles, probably due to the conformational flexibility of the S–S bond; one of them is shown in Figure 2, together with selected metric parameters (full metric data and details related to X-ray data refinement are summarized in Table S2 in the SI). The six-membered ring including the two sulfur atoms shows a twist-boat conformation with (non-crystallographic) C_2 symmetry, to minimize the strain imposed by the disulfide moiety. The average S–S bond length of 2.054 Å is similar to the one found in [1,2]dithiino[3,4-c:6,5-c']dipyridine (where the N-atoms are at the 4,4'-positions, 2.056 Å).[37] The planes of the two pyridine rings in $^{S-S}$bpy are twisted with an average torsion angle of θ = 33° around the central C5–C6 axis. The averaged C–S–S–C torsion angle is about 60°, which is in accordance with the DFT (Density Function Theory) optimized value of 59.2° predicted for $^{S-S}$bpy[13] and experimental values for the related S_2-bridged compound dibenzo(c,e)(1,2)dithiine (60°).[38]

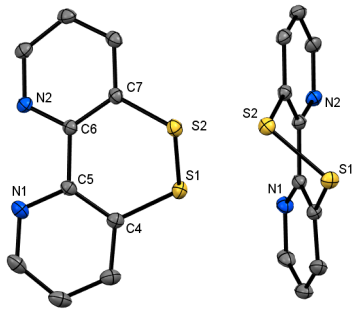

Figure 2. Top view (left) and front view (right; view along the C_2 axis) of the molecular structure of $^{S-S}$bpy (thermal ellipsoids at 50% probability level); hydrogen atoms omitted for clarity. Only one of the two crystallographically independent molecules is shown. Values for the 2nd molecule are given in parenthesis. Selected bond lengths (Å) and -angles (°): S1–S2 2.056(1) (2.051(1)); N1–C5–C6–N2 34.9(1) (31.7(1)), C4–S1–S2–C7 60.8(1) (60.0(1)).

Synthesis and structure of an iridium complex of $^{S-S}$bpy. The cyclometallated iridium(III) complex $[Ir(ppy)_2(^{S-S}bpy)](PF_6)$ (**[1]**PF_6) was synthesized starting from the dimeric precursor $[IrCl(ppy)_2]_2$ and $^{S-S}$bpy in a degassed CH_2Cl_2/CH_3OH mixture (2:1 v/v) at 40 °C under inert atmosphere (Scheme 2). The use of relatively low temperatures prevents the thermal decomposition of $^{S-S}$bpy during the synthesis.[13] After anion exchange with NH_4PF_6 and chromatographic purification, **[1]**PF_6 was obtained as a deep red solid with a yield of 82%.

Scheme 2. Synthesis of the iridium(III) complex **[1]**PF_6.

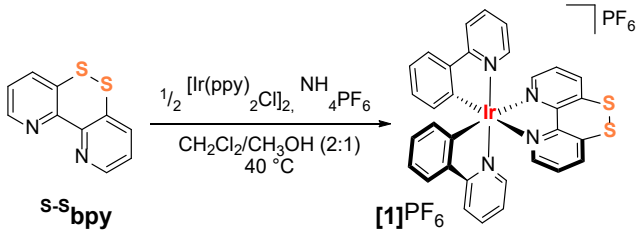

[1]PF_6 was characterized by means of NMR and IR spectroscopies as well as ESI mass spectrometry and combustion analysis (see SI). The ESI(+) mass spectrum shows a dominant peak at m/z = 718, corresponding to the complex cation $[\mathbf{1}]^+$, and the ^{1}H NMR spectrum in CD_3CN shows 11 signals indicative of C_2 symmetry of $[\mathbf{1}]^+$ in solution. Single crystals suitable for X-ray diffraction were obtained by vapor diffusion of diethyl ether into a concentrated acetonitrile solution of **[1]**PF_6. As for the ligand $^{S-S}$bpy, the unit cell contains two crystallographically independent molecules with similar bond lengths and angles; one of them is shown in Figure 3 together with selected metric parameters (see SI for further details).

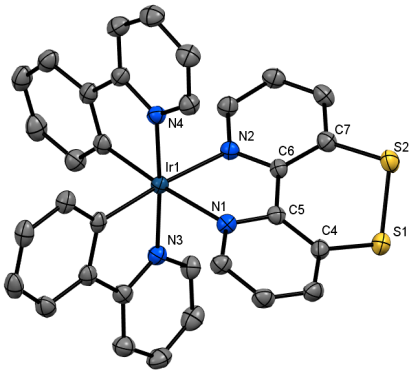

Figure 3. Molecular structure of [**1**]$^+$ (thermal ellipsoids at 50% probability level); hydrogen atoms, solvent molecules and the PF_6 counter ion are omitted for clarity. Only one of the two crystallographically independent molecules is shown. Values for the 2nd molecule are given in parenthesis. Selected bond lengths (Å) and -angles (°): S1–S2 2.045(1) (2.044(1)); C4–S1–S2–C7 56.3(1) (56.3(1)), N1–C5–C6–N2 17.1(1) (17.8(1)).

The iridium center in [**1**]PF_6 is coordinated in pseudo-octahedral geometry by two phenylpyridyl (ppy) ligands and the *N*,*N*'-chelating $^{S–S}$bpy, with the two N-atoms of the ppy ligands in *trans*-position to each other, as expected due to the strong *trans*-influence of the carbanion donors. The N–C–C–N torsion angle in **[1]**$^+$ is reduced to around θ = 18° compared to 33° for free $^{S–S}$bpy, thus maximizing orbital overlap between the donor N-atoms and the metal ion. However, this θ value is the largest among the series of $^{S–S}$bpy complexes reported so far,[17,18] suggesting that [**1**]PF_6 has a more strained $^{S–S}$bpy ligand compared to **A** and **B**. The C–S–S–C torsion angles of around 56° are virtually the same in all three complexes, and also the S–S bond lengths are very similar in the narrow range 2.042-2.048 Å.

Ground-state thermochemistry of disulfide PCET transformations. We have previously determined the PCET thermochemistry of the disulfide/dithiol redox switch in the free $^{S–S}$bpy ligand and **B**, and it was thus interesting to investigate the effect of changing the basicity/size of the metal ion and the ancillary ligand system. To study the redox properties of [**1**]PF_6, cyclic voltammetry (CV) was performed in dry MeCN with 0.2 M ^{n}Bu$_4$NPF_6 as supporting electrolyte and referenced *vs.* the $Fc^{+/0}$ redox couple. In the CV at rt (Figure S7), a quasi-reversible redox process at E = −1.76 V emerged after the first reduction at $E_{p,c}$ = −1.22 V, suggesting that reductive cleavage of the disulfide bond of **[1]**$^+$ leads to decomposition forming [Ir(ppy)$_2$(^{S}bpy)]$^+$ ([**2**]$^+$, Figure 4); sulfur loss from the $^{S–S}$bpy ligand upon reduction was previously observed for **A** and **B**.[17,18] The identity of the decomposition product was confirmed by recording the CV of an independently prepared authentic sample of [**2**]PF_6. The latter was generated by chemical reduction of [**1**]PF_6 with 2 equivalents of cobaltocene at rt (E = −1.3 V vs. $Fc^{+/0}$)[40] and was characterized in solution (see SI for further details and full characterization of [**2**]PF_6).

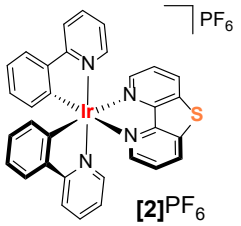

Figure 4. Structural representation of [**2**]PF_6.

In order to slow down decomposition of [**1**]$^+$, the CV measurements were performed at 238 K and 253 K. At these temperatures no evidence for the formation of [**2**]$^+$ on the CV timescale was found down to a scan rate of 0.1 Vs^{-1}. This allows to estimate an unimolecular, all-over reaction rate constant of <0.02 s^{-1} for the decomposition pathway.
The CV data at 238 K (Figure 5) show a reversible oxidation process at $E^{1/2}$ = 0.87 V, which is assigned to the Ir^{IV}/Ir^{III} couple based on the redox properties reported for similar iridium complexes.[41] In the cathodic scan, a reduction process appears at a peak potential of −1.285 V *vs.* $Fc^{+/0}$ (0.1 Vs^{-1}), which shifts cathodically with increasing scan rates. In the reverse scan a broad re-oxidation feature appears at −0.885 V. A plot of the current at different scan rates vs. the square root of the scan rate is linear, which indicates a diffusion-controlled process (Figure S5).

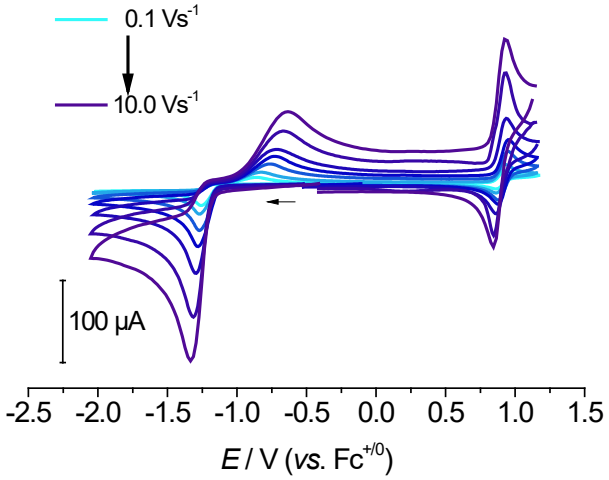

Figure 5. CVs of [**1**]PF_6 recorded at different scan rates in dry MeCN with 0.2 M ^{n}Bu$_4$NPF_6 at 238 K.

The shift of the peak potentials with increasing scan rates, the large separation of the anodic and cathodic process (ΔE = 400-700 mV) and the broad anodic feature point either to an electrochemically irreversible process or an electrochemically reversible process followed by a fast chemical reaction. Since the potential of the reduction wave is similar to the reduction potential of the S–S unit forming the thiolate functions in **A** and **B**, and because the peak current i_p is much larger than the one expected for a 1e$^-$ process, this redox couple can be attributed to the 2e$^-$ reduction of the disulfide bond in the $^{S–S}$bpy ligand of [**1**]$^+$. Moreover, the peak-to-peak separation for the anodic and cathodic waves become smaller when increasing the temperature to 253 K, indicating the recovery of some electrochemical reversibility for this process (Table 1).

Table 1. Redox properties of [1]$^+$ in MeCN in V vs. Fc$^{+/0}$, ν = 0.1 Vs^{-1}. [a] not corrected for the temperature-dependent shift of ferrocene's redox potential.

	E(bpy^{S-S}|bpy^{S2-})		E(Ir$^{(IV\|III)}$)
	$E_{p,c,1}$	$E_{p,a,1}$	$E^{1/2}$
238 K	−1.285	−0.885	0.870
253 K[a]	−1.230	−0.980	0.885

The scan-rate dependent CV data were simulated at both temperatures applying a Butler-Volmer model. The simulated and measured data are in good agreement over a large range of scan-rates. All relevant parameters are given in Table 2, and the overlay of the experimental and simulated data can be found in Figures S3 and S4. The Ir(IV/III) redox process is indeed reversible at 238 and 253 K. The redox potential is slightly affected by the temperature (cf. 15 mV), though the minor shift indicates rather small entropy and enthalpy changes with temperature. The steep slope of the disulfide reduction process indicates a similar reduction potential for both processes, and the broad re-oxidation feature points to an α larger than 0.5. Indeed, the simulations revealed that the second reduction process exhibits a slightly higher potential than the first one at both 238 K and 253 K, hence, potential inversion occurs. Both reduction potentials E_1 and E_2 shift with increasing temperature, though in different directions, which indicates considerable free energy changes with temperature. As expected, the electron transfer rates for the two redox events increase with increasing temperature.

Table 2. Simulated thermodynamic and kinetic parameters for the redox events of [1]$^+$.

	238 K	253 K
E_1 / V	−1.125	−1.17
α_1	0.6	0.6
$k_{s,1}$ / s^{-1}	0.0004	0.0006
E_2 / V	−1.115	−1.08
α_2	0.8	0.8
$k_{s,2}$ / s^{-1}	0.0006	0.0025
E_3 / V	0.885	0.875
α_3	0.5	0.5
$k_{s,3}$ / s^{-1}	0.02	0.03

Since the twice reduced form of **[1]**$^+$, viz. the dithiolate congener **[1]**$^-$, is not thermally stable at room temperature and at high concentrations, UV-vis spectroscopy at −30°C was used for its characterization. Reduction of **[1]**PF_6 with 2 equiv. of cobaltocene at −30°C in MeCN resulted in an increase of absorbance in the range from 320 to 550 nm, with new peaks centered at around 352 nm and a broad absorption at 480 nm (Figure 6, red line). Subsequent protonation (Figure S8) with aliquots of the strong acid [HDMF]OTf (pK_a = 6.1)[42] shows a decrease in the absorbances of both bands at 352 and 480 nm, leading to a spectrum identical to the blue line in Figure 6. No further spectral changes were observed after addition of 1.0 equiv. of [HDMF]OTf, suggesting single protonation and formation of a hydrogen-bonded S–H··S$^-$ unit at the bpy type ligand in **[1H]**. This is in line with the reduction/protonation reported for **B** and similar to the O–H··O$^-$ unit in the analogous bipyridine-diol iridium complex.[18,29]

The pK_a of the S–H··S$^-$ unit in **[1H]** was determined by titration of **[1]**$^-$ with the weaker acid 3,5-dichlorophenol (pK_a(MeCN) = 23.3).[43] Addition of 0.2 equiv. aliquots leads to gradual decrease in absorbance around 352 and 480 nm, as shown in Figure 6. An isosbestic point at 314 nm indicates clean conversion from **[1]**$^-$ to **[1H]**. The obtained titration data at two selected wavelengths were analysed using the method described earlier for deriving the pK_a value[18,44] (details can be found in the SI). A pK_a of 23.5±0.5 was obtained by considering the reported pK_a value of 3,5-dichlorophenol at room temperature. The resulting pK_a value was further bracketed by protonation of **[1]**$^-$ with a weaker acid ([HDBN]$^+$, pK_a = 23.8)[45] and a stronger one (benzoic acid, pK_a = 21.5),[42] which resulted in incomplete conversion or complete protonation with one equivalent of the acid, respectively (Figure S10).

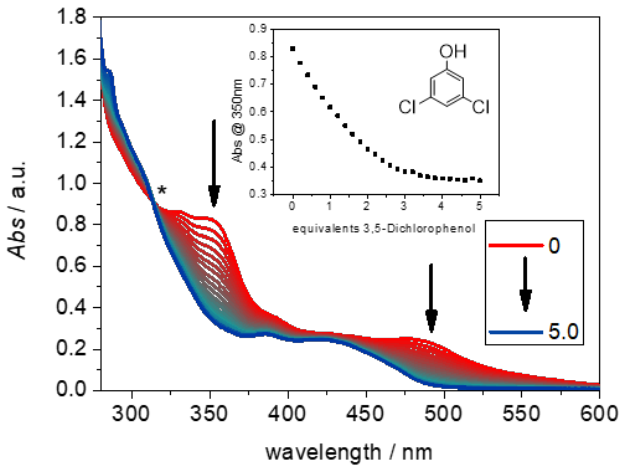

Figure 6. UV-vis spectra of the titration of **[1]**$^-$ with 3,5-dichlorophenol (0 to 5.0 equiv.) in acetonitrile at −30°C (start: red trace, end: blue trace). Inset shows the absorbance followed at 350 nm. The asterisk marks an isosbestic point.

With the potentials (at −20°C: E_1 = −1.17 V and E_2 = −1.08 V) and pK_a-value in hand, the driving forces for both formal hydrogen atom (Equation 1) and hydride (Equation 2) transfer can be calculated using Bordwell's equations[19] with the recently revised[46] value for C_g of 52.6 kcal mol^{-1} and with ΔG(H$^+$\|H$^-$)[19] of 79.6 kcal mol^{-1}.

$$\Delta G(H\bullet) = 1.364\ pK_a + 23.06\ E_1 + C_g = 57.7 \text{ kcal mol}^{-1} \quad (1)$$

$$\Delta G(H^-) = 1.364\ pK_a + 23.06\ E_1 + 23.06\ E_2 + \Delta G(H^+|H^-) = 59.8 \text{ kcal mol}^{-1} \quad (2)$$

The bond dissociation free energy (BDFE; $\Delta G(H^{\bullet})$) of 58 kcal mol^{-1} and the hydricity ($\Delta G(H^{-})$) of 60 kcal mol^{-1} of **[1H]** are very similar to the ones determined for the twice reduced and singly protonated form of **B** (59 and 60 kcal mol^{-1}, respectively), nicely demonstrating the compensating effect of the two free energy contributors: a slightly more cathodic (second) reduction potential of –1.16 V *vs.* a slightly higher pK_a value of 24.7 in case of **B** to give the same free energies as for **[1H]**, despite the fact that the overall charge of the complexes differ. It should be noted that the above values for **B** were determined at rt, whereas the values reported here are not corrected for temperature, but the shift in free energies is only on the order of ±2 kcal mol^{-1}, which likely is within the error of the experiment. The PCET thermochemistry of **[1]**$^{+}$ is summarized in Scheme 3.

Scheme 3. Thermochemistry of **[1]**$^{+}$. Potentials in V vs. $Fc^{+/0}$.

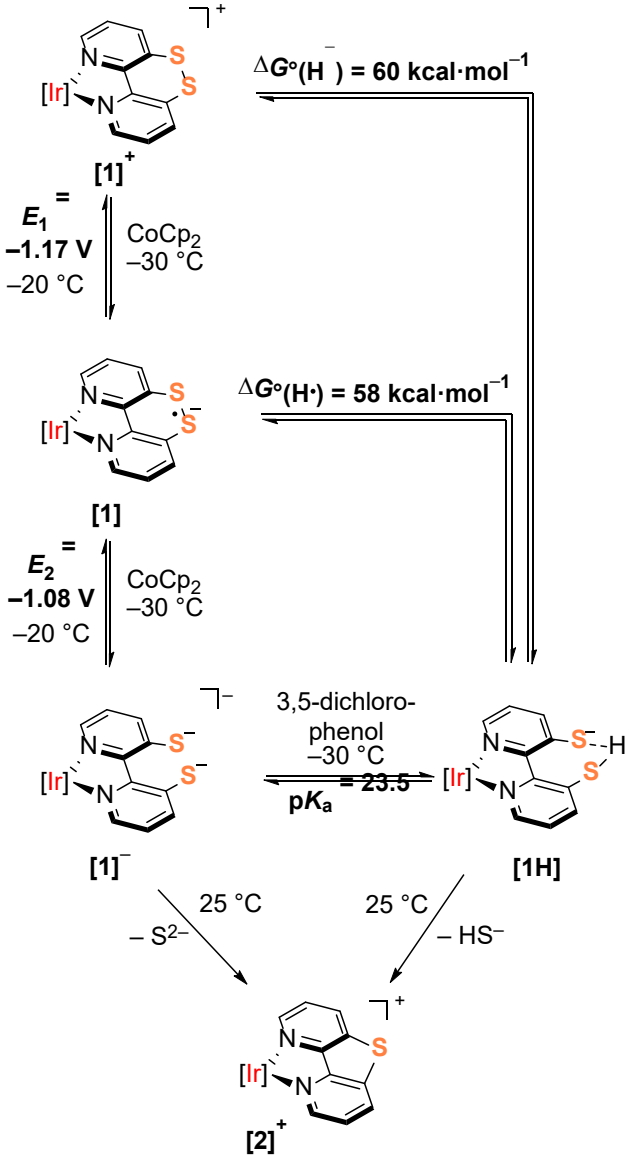

To corroborate the experimentally determined BDFE and hydricity values, reactions of **[1H]** with both an H atom and a hydride acceptor were performed. The stoichiometric reaction of **[1H]** with trityl cation (trityl = triphenylmethyl; $\Delta G(H^{-})$ = 99 kcal mol^{-1})[47] was studied by UV-vis spectroscopy. Addition of 1.0 equiv. of trityl tetrafluoroborate in MeCN at –30 °C to the *in situ* formed **[1H]** (generated by addition of 2.0 equiv of $CoCp_2$ and 1.0 equiv of $[HNEt_3]PF_6$ into the solution of **[1]**PF_6) resulted in the decrease of the UV-vis absorption at 430 nm assigned to **[1H]** (Figure 7). After monitoring the reaction for 5 h, the typical spectral features of **[1]**$^{+}$ are recovered. In a complementary ^{1}H NMR experiment (Figure S24, top), the signal corresponding to triphenylmethane at 4.28 ppm is observed with a spectroscopic yield of 20% in about 12 h (relative to the internal standard 1,3,5-trimethoxybenzene; note that conditions are different in UV-vis and NMR experiments, with concentrations being much higher in the latter). This demonstrates the ability of **[1H]** to act as a hydride donor, thereby forming **[1]**$^{+}$ and triphenylmethane as products of the hydride transfer.

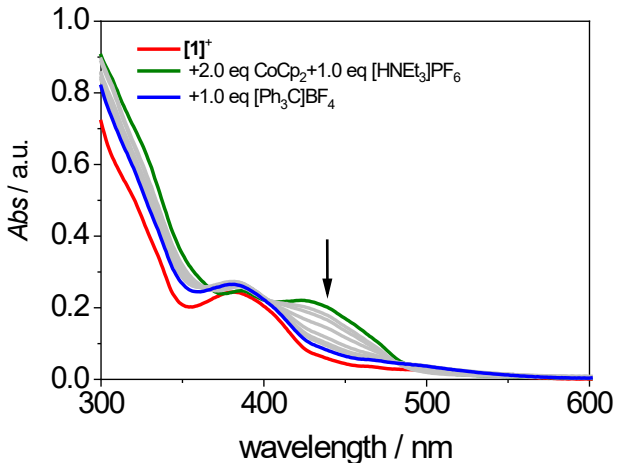

Figure 7. UV-vis spectra during in situ formation of **[1H]** and its reaction with $[Ph_3C]BF_4$ (1.0 equiv.) in MeCN at –30°C over the course of 5 h.

The reaction of **[1H]** with the weaker hydride acceptor $[BIM]PF_6$ ($\Delta G(H^{-})$ = 50 kcal mol^{-1} in MeCN; $[BIM]^{+}$ = 1,3-dimethyl-2-phenyl-1H-benzo[d]imidazol-3-ium)[48] did not lead to any spectral changes, evidencing that no reaction takes place. These results are in line with the experimentally determined hydricity of 60 kcal mol^{-1} of **[1H]**. In addition, H atom transfer reactivity with TEMPO• (2,2',6,6'-tetramethylpiperidine-*N*-hydroxy radical, BDFE = 64 kcal mol^{-1})[49] was probed as well. Reaction of *in situ* formed **[1H]** with TEMPO• at –35 °C showed the signals corresponding to TEMPO–H at 5.25 ppm (Figure S24, bottom) in 43% spectroscopic yield after about 12 h, accompanied by the formation of the characteristic signals for **[2]**$^{+}$; the latter is expected to result from the decomposition of **[1]**$^{-}$ which forms upon disproportionation of **[1]** into **[1]**$^{-}$ and **[1]**$^{+}$. This demonstrates the capability of **[1H]** to serve as a smooth hydride as well as an H atom donor via the peripheral S–H···S^{-} unit.

Photophysical properties. The absorption spectrum (Figure 8, black line) of **[1]**PF_6 in MeCN shows an intense

band (ε = 4.0×10⁴ M⁻¹ cm⁻¹) with an absorption maximum at 265 nm and a shoulder at 260 nm. Furthermore there is a shoulder at >300 nm and a less intense band (ε = 6.5×10³ M⁻¹ cm⁻¹) at λ_{max} = 381 nm as well as a comparatively broad and weak absorption at lower energies. These spectral features are similar to those of the parent complex, $[Ir(ppy)_2(bpy)]^+$.[50]

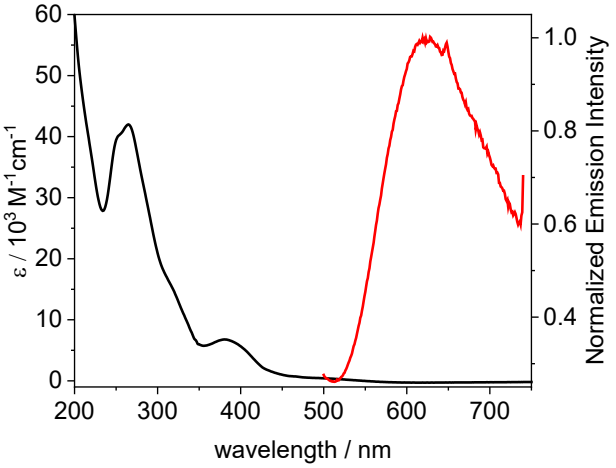

Figure 8. UV-vis absorption (black) and normalized luminescence (red) spectra of **[1]**PF_6 (1.44·10⁻⁵ M) recorded in dry, deaerated MeCN at 293 K. Excitation occurred at 380 nm.

Upon excitation at 380 nm, **[1]**PF_6 in MeCN solution shows a broad, featureless emission with maximum intensity at 627 nm at 293 K (Figure 8, red line), The large shift of 1.29 eV between the lowest absorption band maximum and the emission band maximum is due to the fact that the emission originates from a triplet excited state. Dioxygen quenching experiments show a decrease in emission intensity, confirming that the emission corresponds to phosphorescence. The previously reported complex **A** exhibits an emission peaking at 730 nm.[17] Compared to **A**, the emission maximum of **[1]**PF_6 is shifted hypsochromically by ~0.3 eV, and this can provide a larger driving force for possible reactions with suitable reductive quenchers. In comparison with their respective parent complexes, the emissive states of both **[1]**PF_6 and **A** are lower in energy.

Table 3. Photophysical properties of Ru^{II} complex A and different Ir^{III} complexes in MeCN (phen = 1,10-phenanthroline).

complex	λ_{exc} / nm	λ_{em} / nm	τ / ns	reference
[1]PF_6	380	627	7	this work
[2]PF_6	342	618	416	this work
A	430	730	109	[17]
$[Ir(ppy)_2(bpy)]PF_6$	355	585	430	[50]
$[Ir(ppy)_2(phen)]PF_6$	355	530	1290	[50]

When the luminescence band shown in Figure 8 is tracked kinetically, a bi-exponential decay with a 7 ns component, as well as a 443 ns component are observed (Figures S11 and S12). The short-lived component was probed using the time-correlated single photon counting (TCSPC) technique, where short (ca. 60 ps) and low energy (ca. 10 pJ) laser pulses are applied. The long-lived component was monitored with a setup for longer timescales, which uses a laser with a much higher power output (ca. 10 mJ, see SI for instrumental details).

Even though dual emission has been reported previously for cyclometallated iridium complexes such as $[Ir(ppy)_2(bpy)]^+$,[23] true dual emission is rare and the possibility of emissive trace impurities should be considered carefully.

The steady-state emission spectra of **[1]**PF_6 recorded at 77 K (Figure S15) shows only a single emission band and does not provide further evidence for true dual emission. In principle, different stereoisomers of a given complex can result in different emission properties, and since **[1]**⁺ may exist as different stereoisomers, this possibility cannot be ruled out completely.[51] However, measurements with different excitation laser powers revealed that the long-lived luminescence decay component becomes increasingly pronounced at high excitation powers, indicating the formation of a photo-decomposition product. To elucidate whether this photo-decomposition process leads to the formation of **[2]**⁺, emission spectra and luminescence decays of an authentic sample of **[2]**PF_6 in MeCN were analyzed. The results show that the emission band of **[2]**⁺ indeed peaks at similar emission wavelength (618 nm, Figure S13) as the emission of **[1]**⁺. Furthermore, the luminescence lifetime of **[2]**⁺ (416 ns, Figure S14) is similar to the value of the long-lived component obtained from fitting of the luminescence decay of **[1]**⁺ in MeCN (404 ns, Figure S11), thereby supporting the hypothesis that **[1]**⁺ is not photostable and undergoes light-induced decomposition to **[2]**⁺. UV-vis-spectra recorded before and after irradiation with 200 laser pulses (410 nm, ca. 10 mJ per pulse) of ca. 10 ns duration show no significant differences (Figure S16), suggesting that only a small fraction (ca. 1 nmol, calculated from the change in absorbance upon irradiation, see Figure S16) of **[1]**⁺ undergoes decomposition to **[2]**⁺; the latter presumably emits much more strongly than **[1]**⁺. As a consequence, the overall emission is dominated by the strongly emissive decomposition product **[2]**⁺ whereas **[1]**⁺ features weak emission with a relatively short lifetime of only 7 ns. While decomposition of the $^{S-S}$bpy ligand to give ^{S}bpy was also observed upon electrochemical reduction of ruthenium complex **A** at rt, **A** is photostable and shows well-behaved photochemistry.[17] Possibly, the different photostability of **[1]**⁺ is due to differences in the geometry of the $^{S-S}$bpy ligand of **[1]**⁺ compared to complex **A** (Figure 4). In **[1]**⁺, the twist of the two pyridine rings of $^{S-S}$bpy is the largest among the family of complexes **A** (12.3°), **B** (15.5°), and **[1]**⁺ (17.4°) and this distortion further increases upon photo-excitation according to the DFT-optimized geometries (19.6° and 22.4°, vide infra; Figure 12c, d). It seems plausible that these combined effects promote the formation of the unstrained, planar and robust ^{S}bpy ligand in **[2]**⁺ via sulfur extrusion from **[1]**⁺.

Experimental and theoretical excited state characterization. Figure 9 shows transient difference absorption (TA) spectra of **[1]**PF_6 in MeCN after pump pulse excitation

at 380 nm. Directly after excitation the absorbance change is positive over the entire near UV-vis spectral range with a rather weak band centered at 650 nm, which extends into a region of stronger absorption at wavelengths <520 nm. The drop in optical density between 350 and 450 nm coincides with the ground state absorption band at λ_{max} = 381 nm (see Figure 8) indicating that the TA maximum at 460 nm is likely the result of a superposition of excited state absorption and ground state bleach. The TA signal decays on a ns timescale with no significant change of its spectral shape. This observation suggests the formation of a triplet state within the time resolution of the pump-probe experiment of about 100 fs, characterized by a lifetime of 7 ns consistent with the luminescence decay.

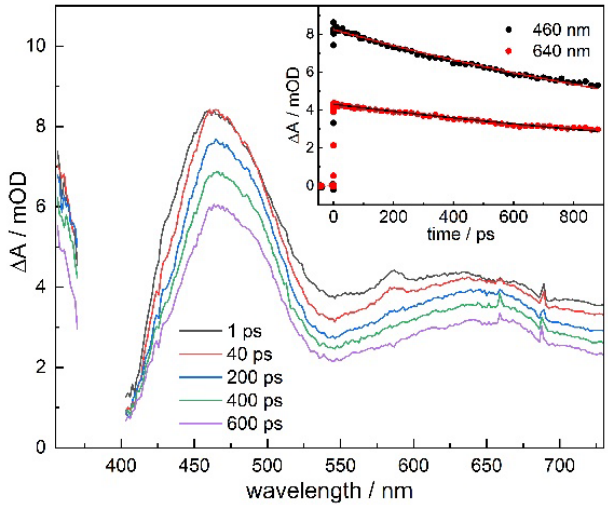

Figure 9. Transient difference absorption spectra of **[1]**PF_6 in MeCN recorded after excitation at 380 nm (regions obscured by scattered light of the pump pulse are cut out). The insert shows time traces at two selected probe wavelengths.

In order to understand the effect of the peripheral disulfide unit on the optical and photophysical properties of **[1]**$^+$, we carried out a set of simulations based on DFT and TD-DFT (Time-Dependent DFT). The same computational approach that already delivered reliable results in previous studies on ruthenium complex **A**[17] has also been employed for **[1]**$^+$. In short, we use B3LYP-D3[52–56] with the LANL2DZ basis set and effective core potential for Ir[57,58] and the 6-311G(d) basis set[59] for the remaining atoms and a polarizable continuum model (PCM)[60] for the implicit solvent MeCN, as implemented within the Gaussian software.[61] The good agreement between the experimental and the computed absorption spectrum of **[1]**$^+$ validates this computational approach (Figure 10). The computed spectrum is obtained within the nuclear ensemble approach via a Wigner sampling[62] of 200 geometries. The spectrum is then decomposed into the different contributions according to charge transfer numbers using the TheoDORE software.[62,63]

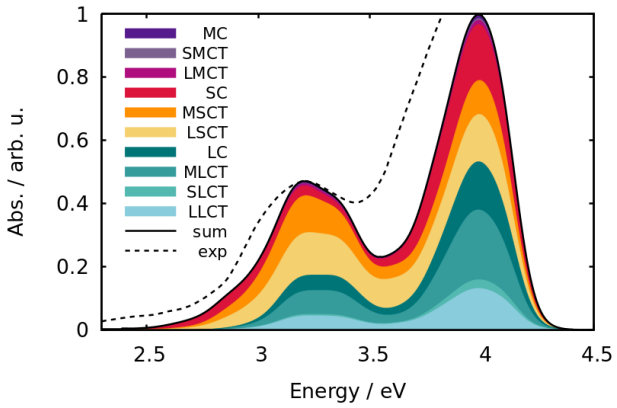

Figure 10. Experimental (dashed line) and calculated (B3LYP-D3/6-311G(d)-LANL2DZ) (black line) absorption spectrum of **[1]**$^+$, with deconvoluted charge-transfer characters. Redish colors indicate charge transfer to the $^{S–S}$bpy ligand, while greenish colors indicate charge transfer to the bpy ligands. Charge transfer to Ir (purple colors) plays a minor role.

We differentiate between (i) metal-centered (MC), (ii) $^{S–S}$bpy ligand to metal charge transfer (SMCT), (iii) unsubstituted bpy ligands to metal charge transfer (LMCT), (iv) $^{S–S}$bpy ligand centered (SC), (v) metal to $^{S–S}$bpy charge transfer (MSCT), (vi) unsubstituted bpy ligands to $^{S–S}$bpy charge transfer (LSCT), (vii) unsubstituted bpy ligand centered (LC), (viii) metal to unsubstituted bpy ligands charge transfer (MLCT), (ix) $^{S–S}$bpy to unsubstituted bpy ligands charge transfer (SLCT), and (x) unsubstituted bpy to unsubstituted bpy charge transfer (LLCT) transitions. As can be seen from Figure 10, the spectrum is of heavily mixed character in all regions.
It is an oversimplification to consider only a single geometry, but this procedure allows to list distinct values and to plot orbitals. Therefore, we focus on the geometry of the lowest minimum of the ground state of **[1]**$^+$ in the following. For this single point geometry, the properties of the lowest ten excited singlet states are listed in Table 4, including excitation energies, associated oscillator strengths and their dominant character.

Table 4. Energy differences to the ground state, oscillator strengths and predominant character of the 10 lowest excited singlet states of [1]$^+$ at the equilibrium ground-state geometry.

State	ΔE / eV	f / a.u.	character
S_1	2.14	0.000	LSCT
S_2	2.71	0.007	SC
S_3	2.84	0.000	MSCT
S_4	2.88	0.030	LSCT
S_5	3.03	0.040	LSCT
S_6	3.06	0.005	LSCT
S_7	3.13	0.053	MLCT
S_8	3.21	0.000	MLCT
S_9	3.21	0.001	LSCT
S_{10}	3.35	0.011	LSCT

Three of the ten states exhibit a relatively high oscillator strength: S_4, S_5, and S_7. For them, the natural transition orbitals are plotted in Figure 11. The S_4 state is denoted as LSCT in Table 4, and this is also evident from the top part of Figure 11, since most of the electron density is transferred from the unsubstituted bpy ligands to the $^{S-S}$bpy ligand. However, also the central metal atom is involved in the transition, which highlights the its mixed character. The situation is very similar for the S_5 state. By contrast, the $^{S-S}$bpy ligand is not involved in the S_7 state. Here, electron density is mostly transferred from the metal to the unsubstituted bpy ligands, and hence labelled as MLCT. Overall, the characters of these states are much more mixed than in complex **A** with a central ruthenium atom. In the latter, a clear separation between an MSCT excitation at lower energies and an MLCT excitation at higher energies has been found, and the excitations clearly start from orbitals located at the metal ion.[17] In contrast, the newly characterized complex $[\mathbf{1}]^+$ with a central Ir ion features excitations which start from orbitals that are much more delocalized over the phenylpyridine ligands and the metal center. This behaviour is typical for cyclometallated Ir complexes.[25]

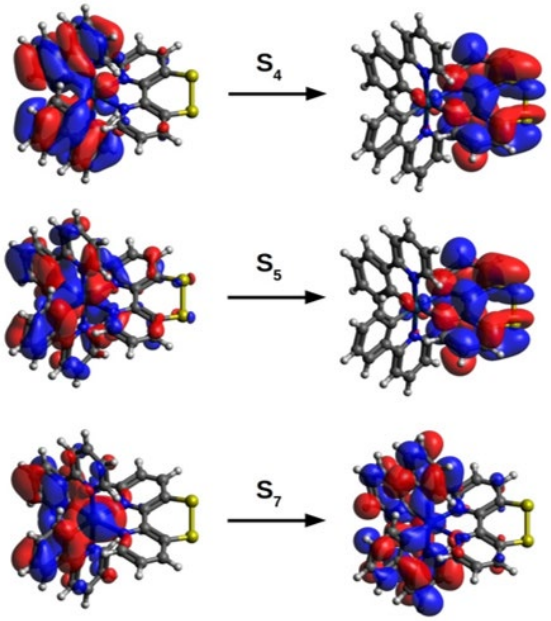

Figure 11. Natural transition orbitals of the states with large oscillator strengths S4, S5, and S7. The contributions of the transitions for respective excited state is above 98% in all cases.

As mentioned above, we hypothesize that the emission observed experimentally for $[\mathbf{1}]^+$ originates from the lowest triplet state (T_1) minimum. The corresponding optimized structure is shown in Figure 12 along with the one for the S_0 minimum. We note that, besides the structure equaling the one found crystallographically for $[\mathbf{1}]PF_6$, a conformer has been identified computationally where the S–S bridge is twisted in the opposite direction, both for the S_0 and the T_1 states (see panels b and d of Figure 12). The energy difference between the conformers is only 0.03 eV or 0.7 kcal mol^{-1} for S_0 and T_1, respectively. Optimization of the transition state between the two S_0 minima gave a barrier of 0.34 eV (7.9 kcal mol^{-1}) for the interconversion between the two conformers.

The most striking difference between the singlet and the triplet minima is the S–S bond length, which is 2.106 Å at S_0 (cf. the crystallographically observed S–S bond length of 2.045(1) Å) and 2.642 Å at T_1 (S_0 twist: 2.105 Å; T_1 twist: 2.627 Å). We assume that the severely stretched S–S bond in the T_1 state provides an effective relaxation channel towards the ground state by transient S–S bond breakage and recombination, which limits the excited state lifetime of $[\mathbf{1}]^+$ to 7 ns. This mechanism can also explain the photo-instability of $[\mathbf{1}]^+$ as a result of incomplete –S• •S- recombination and formation of the sulfur extruded thiophene complex $[\mathbf{2}]^+$.

The computed energy difference between the lowest T_1 minimum and the S_0 at this geometry is 1.66 eV, which corresponds to 747 nm (experimental emission maximum is at 627 nm). The triplet-singlet energy gap might be underestimated in our computational approach, however calculations with other functionals like BP86, which usually yields better singlet-triplet gaps,[64] also provide similar results. Despite this slight disagreement, we assume emission takes place from this lowest T_1 state.

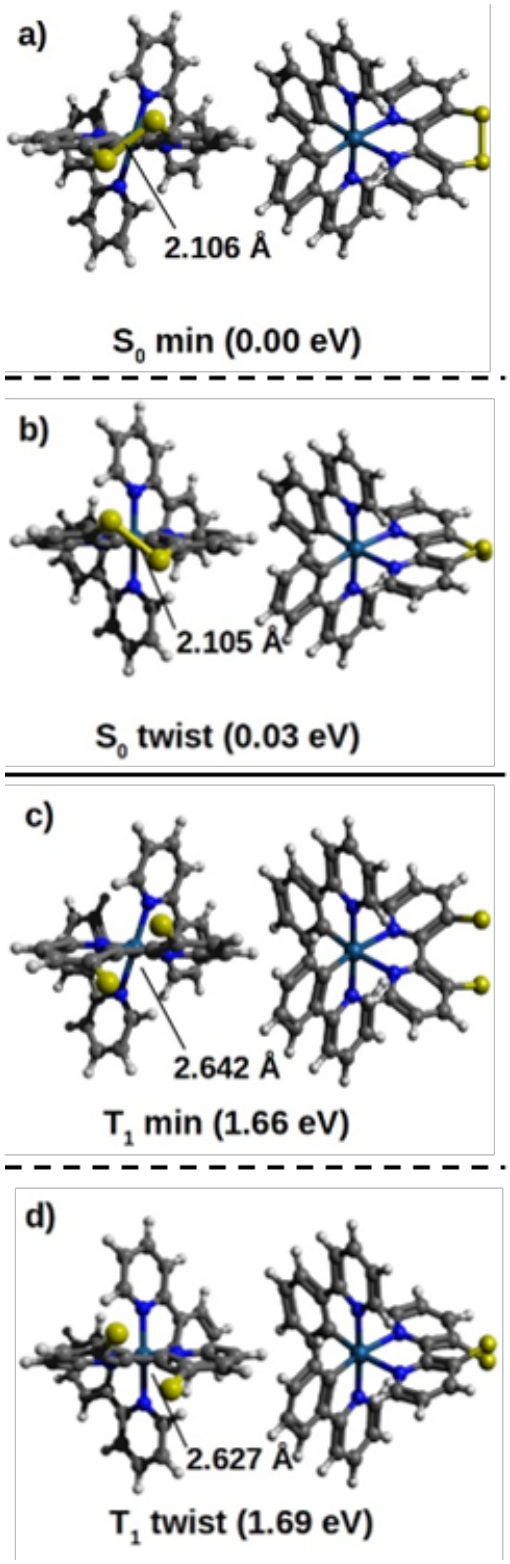

Figure 12. Different conformers (local minima) in the S_0 (a, b) and T_1 (c, d) states and their relative energies from two points of view, respectively. Additionally, the S-S distance is indicated in the different panels. The corresponding .xyz structures are provided as additional SI.

CONCLUSIONS

In this contribution, a new, short and relatively high-yielding synthesis of the sulfurated bipyridine $^{S-S}$bpy is presented, which now allows to conveniently prepare this compound on a gram scale. This will significantly facilitate the use of the promising ligand $^{S-S}$bpy and the exploitation of its disulfide/dithiol-based PCET reactivity.

Complementing the previously reported ruthenium(II) and rhenium(I) complexes **A** and **B**, we present the first iridium complex of $^{S-S}$bpy, **[1]**$^+$, and we have investigated its chemical and photophysical behavior. Whereas **A** is photochemically stable, **[1]**$^+$ seems to gradually decompose upon irradiation. Also the reduced species **[1]**$^-$ and **[1H]** are relatively unstable as they decompose at temperatures above −30°C to give the sulfide-extruded **[2]**$^+$, thereby minimizing electrostatic repulsion and steric strain in the ligand. The redox and acid/base properties of the new system thus had to be examined at −30°C throughout. **[1]**$^+$ shows moderate reduction potentials (−1.17 and −1.08 V at 253 K) and features potential inversion. The reduced species has a pK_a value of 23.5 in MeCN, reminiscent of a rather strong base, which reflects that after S–S bond breakage the two anionic −S$^-$ are constrained in close proximity and have a high tendency to capture a proton with formation of a hydrogen-bonded S–H···S$^-$ unit.

Hydricity and BDFE values of ~60 kcal mol^{-1} have been derived from the reduction potentials and pK_a values, and these are in line with the observed reactivity of **[1H]** with appropriate acceptor molecules, showing that **[1H]** can indeed be used as a proton, H-atom and hydride donor when kept at low temperatures. Despite the different metal ion and coligands as well as the different overall charge of **[1]**$^+$ and the rhenium complex **B**, the thermochemistry of their peripheral disulfide/dithiol moiety ligand turns out to be essentially the same, and key characteristics of the $^{S-S}$bpy ligand such as the potential inversion and basicity of the dithiolate form are retained.

The photophysical properties of **[1]**$^+$ have been investigated in detail by a combination of fs-TA, time-resolved and steady-state emission spectroscopy, and analyzed with the help of DFT calculations. The orange phosphorescence likely originates from a mixed LSCT/MSCT triplet state T_1 that shows a significantly stretched S–S bond and an unexpectedly short lifetime, indicating that the structural responsiveness of the disulfide unit opens a new and effective relaxation channel towards the ground state via transient S–S bond breakage and recombination. It is an interesting perspective to examine the effect of additives that may potentially interact with the disulfide unit, such as protons (pH) or Lewis acidic metal ions, on the photophysical properties. Furthermore, the reduced species **[1]**$^-$ may serve as photoactive metalloligand via its dithiolate function by coordination to a second metal ion, and such studies that aim at using **[1]**$^-$ as a *complex-as-ligand* platform are now pursued in our laboratories.

ASSOCIATED CONTENT

Supporting information is available free of charge via the Internet at http://pubs.acs.org.

General experimental considerations; synthetic protocols and characterization data; additional

electrochemical and thermodynamic data; photochemical data; UV-vis, NMR and IR spectra and crystallographic details. .

AUTHOR INFORMATION

Corresponding Authors

*E-mail: franc.meyer@chemie.uni-goettingen.de
*E-mail: dschwar@mpinat.mpg.de
*E-Mail: leticia.gonzalez@univie.ac.at

Author Contributions

The manuscript was written through contributions of all authors. All authors have given approval to the final version of the manuscript.

Funding Sources

This work was funded by the Deutsche Forschungsgemeinschaft (DFG; German Research Foundation) via projects ME 1313/15-2, SCHW 661/4-2 and GO 1059/8-2 within the SPP 2102 "Light-Controlled Reactivity of Metal Complexes" (project numbers 404391096 and 403837698) and by the Fonds der Chemischen Industrie (Kekulé Fellowship for M.O.). Purchase of the X-ray diffractometer was supported by the Deutsche Forschungsgemeinschaft (DFG) via project number 423268549 (INST 186/1327-1 FUGG) and by the Nds. Ministerium für Wissenschaft und Kultur (MWK).

Notes

Any additional relevant notes should be placed here.

ACKNOWLEDGMENT

The Vienna Scientific Cluster is acknowledged for generous allocation of computer resources.

REFERENCES

(1) Gagliardi, C. J.; Westlake, B. C.; Kent, C. A.; Paul, J. J.; Papanikolas, J. M.; Meyer, T. J. Integrating Proton Coupled Electron Transfer (PCET) and Excited States. *Coord. Chem. Rev.* **2010**, *254* (21–22), 2459–2471. https://doi.org/10.1016/j.ccr.2010.03.001.

(2) Nomrowski, J.; Wenger, O. S. Exploiting Potential Inversion for Photoinduced Multielectron Transfer and Accumulation of Redox Equivalents in a Molecular Heptad. *J. Am. Chem. Soc.* **2018**, *140* (16), 5343–5346. https://doi.org/10.1021/jacs.8b02443.

(3) Lennox, J. C.; Kurtz, D. A.; Huang, T.; Dempsey, J. L. Excited-State Proton-Coupled Electron Transfer: Different Avenues for Promoting Proton/Electron Movement with Solar Photons. *ACS Energy Lett.* **2017**, *2* (5), 1246–1256. https://doi.org/10.1021/acsenergylett.7b00063.

(4) Pannwitz, A.; Wenger, O. S. Proton-Coupled Multi-Electron Transfer and Its Relevance for Artificial Photosynthesis and Photoredox Catalysis. *Chem. Commun.* **2019**, No. 55, 4004–4014. https://doi.org/10.1039/C9CC00821G.

(5) Bürgin, T. H.; Wenger, O. S. Recent Advances and Perspectives in Photodriven Charge Accumulation in Molecular Compounds: A Mini Review. *Energy Fuels* **2021**, *35* (23), 18848–18856. https://doi.org/10.1021/acs.energyfuels.1c02073.

(6) Benson, K. R.; Stash, J.; Moffa, K. L.; Schmehl, R. H.; Dudley, T. J.; Paul, J. J. Ruthenium Complexes with Asymmetric Hydroxy- and Methoxy-Substituted Bipyridine Ligands. *Polyhedron* **2021**, *205*, 115300. https://doi.org/10.1016/j.poly.2021.115300.

(7) Martinez, K.; Benson, K.; Paul, J.; Schmehl, R. H. Photophysics of Ru(II) Complexes with Hydroxylated Diimine Ligands: Photoinduced Electron/Proton Transfer to Anthraquinone. *Polyhedron* **2021**, *207*, 115376. https://doi.org/10.1016/j.poly.2021.115376.

(8) Wenger, O. S. Proton-Coupled Electron Transfer Originating from Excited States of Luminescent Transition-Metal Complexes. *Chem. Eur. J.* **2011**, *17* (42), 11692–11702. https://doi.org/10.1002/chem.201102011.

(9) Polyansky, D.; Cabelli, D.; Muckerman, J. T.; Fujita, E.; Koizumi, T.; Fukushima, T.; Wada, T.; Tanaka, K. Photochemical and Radiolytic Production of an Organic Hydride Donor with a RuII Complex Containing an NAD+ Model Ligand. *Angew. Chem. Int. Ed.* **2007**, *46* (22), 4169–4172. https://doi.org/10.1002/anie.200700304.

(10) Polyansky, D. E.; Cabelli, D.; Muckerman, J. T.; Fukushima, T.; Tanaka, K.; Fujita, E. Mechanism of Hydride Donor Generation Using a Ru(II) Complex Containing an NAD $^+$ Model Ligand: Pulse and Steady-State Radiolysis Studies. *Inorg. Chem.* **2008**, *47* (10), 3958–3968. https://doi.org/10.1021/ic702139n.

(11) Kobayashi, K.; Ohtsu, H.; Nozaki, K.; Kitagawa, S.; Tanaka, K. Photochemical Properties and Reactivity of a Ru Compound Containing an NAD/NADH-Functionalized 1,10-Phenanthroline Ligand. *Inorg. Chem.* **2016**, *55* (5), 2076–2084. https://doi.org/10.1021/acs.inorgchem.5b02390.

(12) Ohtsu, H.; Tanaka, K. An Organic Hydride Transfer Reaction of a Ruthenium NAD Model Complex Leading to Carbon Dioxide Reduction. *Angew. Chem. Int. Ed.* **2012**, *51* (39), 9792–9795. https://doi.org/10.1002/anie.201204348.

(13) Cattaneo, M.; Schiewer, C. E.; Schober, A.; Dechert, S.; Siewert, I.; Meyer, F. 2,2′-Bipyridine Equipped with a Disulfide/Dithiol Switch for Coupled Two-Electron and Two-Proton Transfer. *Chem. Eur. J.* **2018**, *24* (19), 4864–4870. https://doi.org/10.1002/chem.201705022.

(14) Sevier, C. S.; Kaiser, C. A. Formation and Transfer of Disulphide Bonds in Living Cells. *Nat. Rev. Mol. Cell Biol.* **2002**, *3* (11), 836–847. https://doi.org/10.1038/nrm954.

(15) Evans, D. H.; Lehmann, M. W.; Burghart, A.; Little, R. D.; Silvestri, G.; Tallec, A.; Shono, T.; Toftlund, H. Two-Electron Reactions in Organic and Organometallic Electrochemistry. *Acta Chem. Scand.* **1999**, *53*, 765–774. https://doi.org/10.3891/acta.chem.scand.53-0765.

(16) Hall, G. B.; Kottani, R.; Felton, G. A. N.; Yamamoto, T.; Evans, D. H.; Glass, R. S.; Lichtenberger, D. L. Intramolecular Electron Transfer in Bipyridinium Disulfides. *J. Am. Chem. Soc.* **2014**, *136* (10), 4012–4018. https://doi.org/10.1021/ja500087m.

(17) Hua, S.-A.; Cattaneo, M.; Oelschlegel, M.; Heindl, M.; Schmid, L.; Dechert, S.; Wenger, O. S.; Siewert, I.; González, L.; Meyer, F. Electrochemical and Photophysical Properties of Ruthenium(II) Complexes Equipped with Sulfurated Bipyridine Ligands. *Inorg. Chem.* **2020**, *59* (7), 4972–4984. https://doi.org/10.1021/acs.inorgchem.0c00220.

(18) Hua, S.-A.; Paul, L. A.; Oelschlegel, M.; Dechert, S.; Meyer, F.; Siewert, I. A Bioinspired Disulfide/Dithiol Redox Switch in a Rhenium Complex as Proton, H Atom, and Hydride Transfer Reagent. *J. Am. Chem. Soc.* **2021**, *143* (16), 6238–6247. https://doi.org/10.1021/jacs.1c01763.

(19) Wiedner, E. S.; Chambers, M. B.; Pitman, C. L.; Bullock, R. M.; Miller, A. J. M.; Appel, A. M. Thermodynamic Hydricity of Transition Metal Hydrides. *Chem. Rev.* **2016**, *116* (15), 8655–8692. https://doi.org/10.1021/acs.chemrev.6b00168.

(20) Heindl, M.; Hongyan, J.; Hua, S.-A.; Oelschlegel, M.; Meyer, F.; Schwarzer, D.; González, L. Excited-State Dynamics of $[Ru(^{S-S}Bpy)(Bpy)_2]^{2+}$ to Form Long-Lived Localized Triplet States. *Inorg. Chem.* **2021**, *60* (3), 1672–1682. https://doi.org/10.1021/acs.inorgchem.0c03163.

(21) Goldsmith, J. I.; Hudson, W. R.; Lowry, M. S.; Anderson, T. H.; Bernhard, S. Discovery and High-Throughput Screening of Heteroleptic Iridium Complexes for Photoinduced Hydrogen Production. *J. Am. Chem. Soc.* **2005**, *127* (20), 7502–7510. https://doi.org/10.1021/ja0427101.

(22) Colombo, M. G.; Hauser, A.; Guedel, H. U. Evidence for Strong Mixing between the LC and MLCT Excited States in Bis(2-Phenylpyridinato-C2,N')(2,2'-Bipyridine)Iridium(III). *Inorg. Chem.* **1993**, *32* (14), 3088–3092. https://doi.org/10.1021/ic00066a020.

(23) King, K. A.; Watts, R. J. Dual Emission from an Ortho-Metalated Iridium(III) Complex. *J. Am. Chem. Soc.* **1987**, *109* (5), 1589–1590. https://doi.org/10.1021/ja00239a060.

(24) Wu, S.-H.; Ling, J.-W.; Lai, S.-H.; Huang, M.-J.; Cheng, C. H.; Chen, I.-C. Dynamics of the Excited States of [Ir(Ppy)2bpy]+ with Triple Phosphorescence. *J. Phys. Chem. A* **2010**, *114* (38), 10339–10344. https://doi.org/10.1021/jp102264q.

(25) Lowry, M. S.; Bernhard, S. Synthetically Tailored Excited States: Phosphorescent, Cyclometalated Iridium(III) Complexes and Their Applications. *Chem. Eur. J.* **2006**, *12* (31), 7970–7977. https://doi.org/10.1002/chem.200600618.

(26) Ladouceur, S.; Zysman-Colman, E. A Comprehensive Survey of Cationic Iridium(III) Complexes Bearing Nontraditional Ligand Chelation Motifs. *Eur. J. Inorg. Chem.* **2013**, No. 17, 2985–3007. https://doi.org/10.1002/ejic.201300171.

(27) Shaw, M. H.; Twilton, J.; MacMillan, D. W. C. Photoredox Catalysis in Organic Chemistry. *J. Org. Chem.* **2016**, *81* (16), 6898–6926. https://doi.org/10.1021/acs.joc.6b01449.

(28) Nazeeruddin, Md. K.; Humphry-Baker, R.; Berner, D.; Rivier, S.; Zuppiroli, L.; Graetzel, M. Highly Phosphorescence Iridium Complexes and Their Application in Organic Light-Emitting Devices. *J. Am. Chem. Soc.* **2003**, *125* (29), 8790–8797. https://doi.org/10.1021/ja021413y.

(29) Suzuki, Y.; Mizuno, I.; Tabei, Y.; Fujioka, Y.; Shinozaki, K.; Sugaya, T.; Ishihara, K. Highly Selective Aluminum(III) Ion Sensing with Luminescent Iridium(III) Complexes Bearing a Distorted 2,2′-Bipyridine-3,3′-Diol Moiety Utilizing a Rigidified Seven-Membered Chelate Ring. *Inorg. Chem.* **2019**, *58* (15), 9663–9671. https://doi.org/10.1021/acs.inorgchem.9b00373.

(30) DeRosa, M. C.; Hodgson, D. J.; Enright, G. D.; Dawson, B.; Evans, C. E. B.; Crutchley, R. J. Iridium Luminophore Complexes for Unimolecular Oxygen Sensors. *J. Am. Chem. Soc.* **2004**, *126* (24), 7619–7626. https://doi.org/10.1021/ja049872h.

(31) Witt, D. Recent Developments in Disulfide Bond Formation. *Synthesis* **2008**, *2008* (16), 2491–2509. https://doi.org/10.1055/s-2008-1067188.

(32) Zhang, B.; Breslow, R. Ester Hydrolysis by a Catalytic Cyclodextrin Dimer Enzyme Mimic with a Metallobipyridyl Linking Group. *J. Am. Chem. Soc.* **1997**, *119* (7), 1676–1681. https://doi.org/10.1021/ja963769d.

(33) Lloyd-Jones, G.; Moseley, J.; Renny, J. Mechanism and Application of the Newman-Kwart O→S Rearrangement of *O* -Aryl Thiocarbamates. *Synthesis* **2008**, *2008* (5), 661–689. https://doi.org/10.1055/s-2008-1032179.

(34) Nishide, K.; Ohsugi, S.; Miyamoto, T.; Kumar, K.; Node, M. Development of Odorless Thiols and Sulfides and Their Applications to Organic Synthesis. *Monatsh. Chem.* **2004**, *135* (2), 189–200. https://doi.org/10.1007/s00706-003-0122-1.

(35) Zoltewicz, J. A.; Dill, C. D. Inter-Ring Directed Ortho Lithiation by the 2-Pyridyl Group in Bipyridines. *Tetrahedron* **1996**, *52* (46), 14469–14474. https://doi.org/10.1016/0040-4020(96)00892-7.

(36) Cossu, S.; Delogu, G.; Fabbri, D.; Maglioli, P. A Rapid Preparation of 2,2′-Dimercaptobiphenyl. *Org. Prep. Proc. Int.* **1991**, *23* (4), 455–457. https://doi.org/10.1080/00304949109458237.

(37) Benniston, A. C.; Hagon, J.; He, X.; Yang, S.; Harrington, R. W. Spring Open Two-plus-Two Electron Storage in a Disulfide-Strapped Methyl Viologen Derivative. *Org. Lett.* **2012**, *14* (2), 506–509. https://doi.org/10.1021/ol203099h.

(38) Aucott, S. M.; Milton, H. L.; Robertson, S. D.; Slawin, A. M. Z.; Woollins, J. D. Crystal Structures of Dibenzo[Ce]-1,2-Dithiine and Its Related Oxides. *Heteroatom Chem.* **2005**, *16* (5), 346–351. https://doi.org/10.1002/hc.20101.

(39) Lowry, M. S.; Hudson, W. R.; Pascal, R. A.; Bernhard, S. Accelerated Luminophore Discovery through Combinatorial Synthesis. *J. Am. Chem. Soc.* **2004**, *126* (43), 14129–14135. https://doi.org/10.1021/ja047156+.

(40) Connelly, N. G.; Geiger, W. E. Chemical Redox Agents for Organometallic Chemistry. *Chem. Rev.* **1996**, *96* (2), 877–910. https://doi.org/10.1021/cr940053x.

(41) Bevernaegie, R.; Wehlin, S. A. M.; Elias, B.; Troian-Gautier, L. A Roadmap Towards Visible Light Mediated Electron Transfer Chemistry with Iridium(III) Complexes. *ChemPhotoChem* **2021**, *5* (3), 217–234. https://doi.org/10.1002/cptc.202000255.

(42) McCarthy, B. D.; Martin, D. J.; Rountree, E. S.; Ullman, A. C.; Dempsey, J. L. Electrochemical Reduction of Brønsted Acids by Glassy Carbon in Acetonitrile—Implications for Electrocatalytic Hydrogen Evolution. *Inorg. Chem.* **2014**, *53* (16), 8350–8361. https://doi.org/10.1021/ic500770k.

(43) Eckert, F.; Leito, I.; Kaljurand, I.; Kütt, A.; Klamt, A.; Diedenhofen, M. Prediction of Acidity in Acetonitrile Solution with COSMO-RS. *J. Comput. Chem.* **2009**, *30* (5), 799–810. https://doi.org/10.1002/jcc.21103.

(44) Barman, S. K.; Jones, J. R.; Sun, C.; Hill, E. A.; Ziller, J. W.; Borovik, A. S. Regulating the Basicity of Metal–Oxido Complexes with a Single Hydrogen Bond and Its Effect on C–H Bond Cleavage. *J. Am. Chem. Soc.* **2019**, *141* (28), 11142–11150. https://doi.org/10.1021/jacs.9b03688.

(45) Kovačević, B.; Maksić, Z. B. Basicity of Some Organic Superbases in Acetonitrile. *Org. Lett.* **2001**, *3* (10), 1523–1526. https://doi.org/10.1021/ol0158415.

(46) Agarwal, R. G.; Wise, C. F.; Warren, J. J.; Mayer, J. M. Correction to Thermochemistry of Proton-Coupled Electron Transfer Reagents and Its Implications. *Chem. Rev.* **2021**, acs.chemrev.1c00791. https://doi.org/10.1021/acs.chemrev.1c00791.

(47) Zhang, X.-M.; Bruno, J. W.; Enyinnaya, E. Hydride Affinities of Arylcarbenium Ions and Iminium Ions in Dimethyl Sulfoxide and Acetonitrile. *J. Org. Chem.* **1998**, *63* (14), 4671–4678. https://doi.org/10.1021/jo980120d.

(48) Ilic, S.; Alherz, A.; Musgrave, C. B.; Glusac, K. D. Thermodynamic and Kinetic Hydricities of Metal-Free Hydrides. *Chem. Soc. Rev.* **2018**, *47* (8), 2809–2836. https://doi.org/10.1039/C7CS00171A.

(49) Warren, J. J.; Tronic, T. A.; Mayer, J. M. Thermochemistry of Proton-Coupled Electron Transfer Reagents and Its Implications. *Chem. Rev.* **2010**, *110* (12), 6961–7001. https://doi.org/10.1021/cr1000858k.

(50) Costa, R. D.; OrtÃ-, E.; Bolink, H. J.; Graber, S.; Schaffner, S.; Neuburger, M.; Housecroft, C. E.; Constable, E. C. Archetype Cationic Iridium Complexes and Their Use in Solid-State Light-Emitting Electrochemical Cells. *Adv. Funct. Mater.* **2009**, *19* (21), 3456–3463. https://doi.org/10.1002/adfm.200900911.

(51) Takaishi, K.; Nakatsuka, Y.; Asano, H.; Yamada, Y.; Ema, T. Ruthenium Complexes Bearing Axially Chiral Bipyridyls: The Mismatched Diastereomer Showed Red Circularly Polarized Phosphorescence. *Chem. Eur. J.* **2021**, chem.202104212. https://doi.org/10.1002/chem.202104212.

(52) Becke, A. D. Density-functional Thermochemistry. III. The Role of Exact Exchange. *J. Chem. Phys.* **1993**, *98* (7), 5648–5652. https://doi.org/10.1063/1.464913.

(53) Lee, C.; Yang, W.; Parr, R. G. Development of the Colle-Salvetti Correlation-Energy Formula into a Functional of the Electron Density. *Phys. Rev. B* **1988**, *37* (2), 785–789. https://doi.org/10.1103/PhysRevB.37.785.

(54) Vosko, S. H.; Wilk, L.; Nusair, M. Accurate Spin-Dependent Electron Liquid Correlation Energies for Local Spin Density Calculations: A Critical Analysis. *Can. J. Phys.* **1980**, *58* (8), 1200–1211. https://doi.org/10.1139/p80-159.

(55) Stephens, P. J.; Devlin, F. J.; Chabalowski, C. F.; Frisch, M. J. Ab Initio Calculation of Vibrational Absorption and Circular Dichroism Spectra Using Density Functional Force Fields. *J. Phys. Chem.* **1994**, *98* (45), 11623–11627. https://doi.org/10.1021/j100096a001.

(56) Grimme, S.; Antony, J.; Ehrlich, S.; Krieg, H. A Consistent and Accurate *Ab Initio* Parametrization of Density Functional Dispersion Correction (DFT-D) for the 94 Elements H-Pu. *J. Chem. Phys.* **2010**, *132* (15), 154104. https://doi.org/10.1063/1.3382344.

(57) Hay, P. J.; Wadt, W. R. *Ab Initio* Effective Core Potentials for Molecular Calculations. Potentials for the Transition Metal Atoms Sc to Hg. *J. Chem. Phys.* **1985**, *82* (1), 270–283. https://doi.org/10.1063/1.448799.

(58) Hay, P. J.; Wadt, W. R. *Ab Initio* Effective Core Potentials for Molecular Calculations. Potentials for K to Au Including the Outermost Core Orbitals. *J. Chem. Phys.* **1985**, *82* (1), 299–310. https://doi.org/10.1063/1.448975.

(59) Krishnan, R.; Binkley, J. S.; Seeger, R.; Pople, J. A. Self-consistent Molecular Orbital Methods. XX. A Basis Set for Correlated Wave Functions. *J. Chem. Phys.* **1980**, *72* (1), 650–654. https://doi.org/10.1063/1.438955.

(60) Tomasi, J.; Mennucci, B.; Cammi, R. Quantum Mechanical Continuum Solvation Models. *Chem. Rev.* **2005**, *105* (8), 2999–3094. https://doi.org/10.1021/cr9904009.

(61) M. J. Frisch, G. W. Trucks, H. B. Schlegel, G. E. Scuseria, M. A. Robb, J. R. Cheeseman, G. Scalmani, V. Barone, G. A. Petersson, H. Nakatsuji, X. Li, M. Caricato, A. V. Marenich, J. Bloino, B. G. Janesko, R. Gomperts, B. Mennucci, H. P. Hratchian, J. V. Ortiz, A. F. Izmaylov, J. L. Sonnenberg, D. Williams-Young, F. Ding, F. Lipparini, F. Egidi, J. Goings, B. Peng, A. Petrone, T. Henderson, D. Ranasinghe, V. G. Zakrzewski, J. Gao, N. Rega, G. Zheng, W. Liang, M. Hada, M. Ehara, K. Toyota, R. Fukuda, J. Hasegawa, M. Ishida, T. Nakajima, Y. Honda, O. Kitao,

H. Nakai, T. Vreven, K. Throssell, J. A. Montgomery, Jr., J. E. Peralta, F. Ogliaro, M. J. Bearpark, J. J. Heyd, E. N. Brothers, K. N. Kudin, V. N. Staroverov, T. A. Keith, R. Kobayashi, J. Normand, K. Raghavachari, A. P. Rendell, J. C. Burant, S. S. Iyengar, J. Tomasi, M. Cossi, J. M. Millam, M. Klene, C. Adamo, R. Cammi, J. W. Ochterski, R. L. Martin, K. Morokuma, O. Far-kas, J. B. Foresman, and D. J. Fox. *Gaussian 16, Revision A.03*; Gaussian Inc.: Wallingford CT, 2016.

(62) Mai, S.; Marquetand, P.; González, L. Surface Hopping Molecular Dynamics. In *Quantum Chemistry and Dynamics of Excited States*; John Wiley & Sons, Ltd, 2020; pp 499–530. https://doi.org/10.1002/9781119417774.ch16.

(63) Plasser, F. TheoDORE: A Toolbox for a Detailed and Automated Analysis of Electronic Excited State Computations. *J. Chem. Phys.* **2020**, *152* (8), 084108. https://doi.org/10.1063/1.5143076.

(64) Atkins, A. J.; Talotta, F.; Freitag, L.; Boggio-Pasqua, M.; González, L. Assessing Excited State Energy Gaps with Time-Dependent Density Functional Theory on Ru(II) Complexes. *J. Chem. Theory Comput.* **2017**, *13* (9), 4123–4145. https://doi.org/10.1021/acs.jctc.7b00379.

Insert Table of Contents artwork here

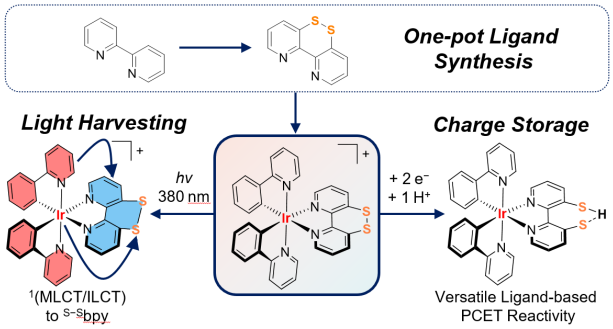

TOC Synopsis

An improved one-pot synthetic protocol for the disulfide-decorated bipyridine ligand $^{S-S}$bpy has been developed, and a new cyclometallated iridium(III) complex of $^{S-S}$bpy has been synthesized that features mixed charge-transfer excitations towards the sulfurated ligand, as shown by TD-DFT calculations. Storage of one proton and two electrons is possible at the disulfide moiety, which can later be released as either proton, H atom or hydride in versatile ligand-based PCET reactivity.